

Nonlinear Forced Response of Plasmonic Nanostructures

Kobi Frischwasser,¹ Kobi Cohen,¹ Shai Tsesses¹,¹ Shimon Dolev,¹ Gilad Rosenblatt²,² and Guy Bartal¹

¹*Technion–Israel Institute of Technology, Haifa, Israel*

²*P.O. Box 31415, Haifa, Israel*



(Received 12 June 2021; accepted 7 January 2022; published 7 March 2022)

Incorporating optical surface waves in nonlinear processes unlocks unique and sensitive nonlinear interactions wherein highly confined surface states can be accessed and explored. Here, we unravel the rich physics of modal-nonmodal state pairs of short-range surface plasmons in thin metal films by leveraging “dark nonlinearity”—a nonradiating nonlinear source. We control and observe the nonlinear forced response of these modal-nonmodal pairs and present nonlinearly mediated direct access to nonmodal plasmons in a lossless regime. Our study can be generalized to other forms of surface waves or optical nonlinearities, toward on-chip nonlinearly controlled nanophotonic devices.

DOI: [10.1103/PhysRevLett.128.103901](https://doi.org/10.1103/PhysRevLett.128.103901)

Two years after the first demonstration of the laser, Bloembergen and Pershan established the theoretical framework for nonlinear generation of light at the interface between a linear and nonlinear media [1]. In their pioneering work, they generalized Snell’s law of refraction and reflection to nonlinear fields, by solving Maxwell’s equations in a nonlinear medium subjected to the proper boundary conditions at the interface. This analysis laid the foundations for the versatile research of surface and bulk optical nonlinearities at the interface of dielectric and metallic media [2–7].

In 1974, the important role of surface plasmon polaritons (SPPs) in enhanced second harmonic generation emanating from a thin metallic film, was first elucidated [8], showing that the bound nature of SPPs may give rise to an increased field localization at the interface of metals and therefore enable boosted nonlinear conversion efficiency. The highly confined electric fields in plasmonic nanostructures have since been exploited for enhanced harmonic generation [9–11], nonlinear phase-control [12], nonlinear holography [13], nonlinear negative refraction [14], and nonlinear near-field microscopy [15], along with a multitude of unique nonlinear phenomena.

While accessing SPPs by linear means requires specialized coupling schemes such as corrugated surfaces or high-index substrates [16,17], Palomba *et al.* were the first to recognize that a nonlinear four-wave-mixing process in metals can be used to directly excite SPPs [18]. This novel coupling scheme initiated the research of nonlinearly assisted coupling between propagating waves and surface waves [19–22].

Nonlinear surface wave excitation exhibits a rich complexity when the metal film becomes sufficiently thin, such that it can no longer be considered semi-infinite for SPPs. In such thin nanostructures, surface modes residing at each boundary of the film hybridize and form two different sets

of solutions, known as short-range (SR) and long-range (LR) SPPs, strongly and weakly confined, respectively [17]. In particular, for an asymmetric insulator-metal-insulator (IMI) nanostructure, short-range SPPs localize predominantly at the interface with the high-index insulator, while long-range SPPs localize at the interface with the low-index insulator [23–25].

Asymmetric IMI structures were instrumental in exploring the *forced* response of plasmonic systems, and illustrated how—in the presence of a light source—plasmonic states come in pairs made of two distinct variants: discrete resonant modes and a continuum of nonmodal states representing the forced optical response of a structure and characterized as an antiresonance in the reflection coefficient [26]. While the long-range resonant-antiresonant plasmon pair were observed using a high-index coupling prism, its short-range plasmonic counterpart is highly confined to the metal-prism interface and cannot be accessed this way. Approaching these high-momentum buried states can enable the sensitive examination of the high-index insulator, promoting applications such as biological inspection or high-resolution microscopy.

However, direct access to these states requires placing a nonradiating (“dark”) evanescent source in close proximity to the interface of the low-index insulator and the metal thus applying decaying fields into the metal. One possible way to linearly obtain such high momentum fields is corrugating the surface of the metal. However, experiments demonstrate that such a coupling scheme mostly excites the modal SR plasmonic state, while the nonmodal state is restricted to the source location and so was never observed to the best of our knowledge.

Here, we present the first nonlinear control over the high-momentum regime of the forced optical response of thin films, comprising both modal and nonmodal degrees of freedom of short-range surface plasmon polaritons.

By generating a nonradiating “dark nonlinearity,” acting as a nonlinear source of evanescent fields on a thin metallic film, we access and measure the modal-nonmodal state pairs manifested as resonant and antiresonant short-range plasmons. We find that small variations in the metal film thickness drastically change the interrelations of these modal and nonmodal states and identify the optimal conditions for the nonlinear source to provide a direct access to nonmodal short-range plasmons in a lossless regime.

Our experimental results, accompanied by complex-plane analysis, open new scientific directions where nanophotonic systems are dominated by nonlinear modal and nonmodal states. Such control has recently become important for applications such as low-loss propagation in optical fibers [27,28] and antilasing [29] and could lead to accurate nonlinear control and functionalities for on-chip nanophotonic devices.

In an asymmetrical IMI configuration, each of the adjacent metal-dielectric interfaces contributes a resonant and an antiresonant plasmonic field solution to the optical response. Such paired excitations manifest as peak-and-dip signatures in the reflection coefficient, that track the different dispersion relations of these two types of field solutions [26]. An exemplary system is a 40 nm gold film atop a glass substrate, illuminated from the air side, whose reflection diagram is illustrated in Fig. 1(a). Both the resonant long-range and short-range plasmons appear as reflection maxima, while the antiresonant short-range plasmon appears as a minimum. All these excitations lie outside the air light cone, indicating that the impinging wave vectors required to excite them are evanescent.

Note that unlike its resonant counterpart, the antiresonant long-range plasmon is inaccessible from the air side. This is a general response of a three-layer system comprising two evanescently coupled metal-dielectric interfaces. The antiresonant state corresponds to nullified reflection that

emerges when the contribution of the single-interface SPP propagating along the interface on the side of the source is suppressed by the sum of the incoming field and the remaining response contributed by the second SPP propagating along the farther interface. Consequently, the interface closest to the source cannot directly contribute to the antiresonant state [26]. Hence, each of the two possible antiresonant states is excited only when placing the source at the appropriate side: the LR antiresonant state can only be excited from the high-index side, and the SR antiresonant state—only from the air side. From energy conservation, both antiresonant states decay away from the source beyond the film. The LR antiresonant state decays into the air, while the SR antiresonant state decays into the high-index dielectric. In case of a semi-infinite metal there is only one interface, so the condition for an antiresonant state is generally not met. It is by virtue of the second interface in the system that such a state can be excited [30].

A more complete physical picture is attained by fixing the wavelength and expanding the reflection diagram to complex wave vectors. In this representation, one can clearly associate the short-range resonant and antiresonant plasmons with the zero-pole pair highlighted in Fig. 1(b) (for 667 nm wavelength). Their corresponding field profiles are shown in the inset. Although the short-range resonant SPPs decays into both dielectrics, the antiresonant solution can grow exponentially into the air side, depending on the sign of the imaginary component of the transverse wave vector. This one-sided growth indicates that more power is incident by the source than is dissipated by the structure.

However, while both resonant and antiresonant long-range plasmons can be linearly addressed by illuminating through a high-index prism, far-field detection of the short-range pole-zero pair is impossible this way and, therefore, requires illumination from the air side which should be accompanied by a compensation of the excess momentum.

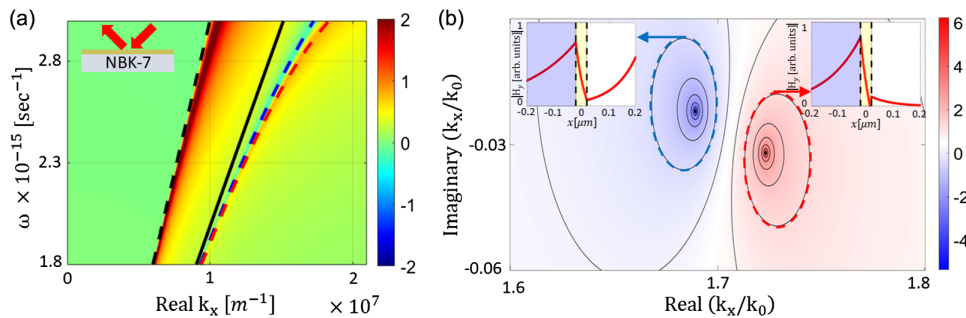


FIG. 1. The linear forced response of resonant and antiresonant short-range plasmons. (a) Real part of the dispersion curves for the resonant (dashed red) and antiresonant (dashed blue) short-range plasmons as a function of angular frequency ω and longitudinal wave vector k_x , over the calculated field amplitude reflection coefficient (log scale) for a 40 nm gold film. Black solid and dashed lines represent the glass and air light lines, respectively. Inset: illustration of the reflection process from a thin gold film atop a glass substrate. (b) In the complex wave-vector domain (log scale), the short-range resonant and antiresonant plasmons at a wavelength of 667 nm appear as a reflection pole (red) and zero (blue), respectively. Their calculated magnetic field amplitudes are plotted in the inset. The blue, yellow, and white areas of the plot represent the substrate, metallic, and air layers of the asymmetric IMI configuration, respectively.

For these purposes, we employ the inherent optical nonlinearity in metals [3,5] to access the large wave vectors of short-range plasmons with freely propagating light. In principle, nonlinear polarization is generated through parametric processes like sum-frequency generation and four-wave mixing [31], coherently mixing the frequency and momentum of different intense waves [2,3,8,32]. Here, the thin gold film can generate a sufficiently strong nonlinear response via the parametric process of partially degenerate four-wave mixing (PDFWM) so as to excite short-range plasmons. The conservation of energy and momentum for PDFWM takes the form of

$$\omega_{\text{nl}} = 2\omega_a - \omega_b, \quad (1a)$$

$$k_{x,\text{nl}} = 2k_{x,a} - k_{x,b}, \quad (1b)$$

where $k_{x,i} = k_{0,i} \sin \theta_i$ is the in-plane component of the wave vector, $k_{0,i} = 2\pi/\lambda_i$ is the free-space wave number at wavelength λ_i , ω_i is the angular frequency, θ_i is the angle of incidence, and the subscript i denotes the pump (a), signal (b), or nonlinearly generated (nl) waves. The requirement on the wave vector of the nonlinearly generated wave is therefore

$$k_{x,\text{nl}} = \text{Re}[k_{\text{SR}}(\omega_{\text{nl}})] > n_{\text{prism}}(\omega_{\text{nl}})k_{0,\text{nl}}, \quad (2)$$

where $n_{\text{prism}}(\omega_{\text{nl}})$ is the refractive index of the glass substrate at the nonlinear angular frequency ω_{nl} and k_{SR} is the in-plane wave vector of the nonlinearly generated short-range plasmons.

We calculate the emerging nonlinear field using a nonlinear transfer matrix method, imposing the appropriate boundary conditions [33–35]. Its detailed step-by-step derivation can be found in Supplemental Material [36].

Extending the analysis to the complex reciprocal plane reveals the behavior of the nonlinearly generated resonant (emission pole) and antiresonant (emission zero) short-range plasmons exemplified for three metallic widths (which were experimentally investigated) Figs. 2(a)–2(c) and in a continuous manner Fig. 2(d). It should be noted that at a specific film thickness of about 62 nm, the nonlinear source completely compensates for the Ohmic losses of the antiresonant short-range plasmon. This is indicated by its purely real wave vector, as its associated reflection zero crosses the real axis [Fig. 2(c)]. At that thickness, the nonlinearity enables a direct access to the antiresonant short-range plasmon, portrayed by the narrowest possible dip. It is important to note that a linear source in this configuration cannot provide the necessary conditions for the compensation of the Ohmic losses (see Supplemental Material [36]).

To study the nonlinear behavior in such systems, we use two experimental schemes in which nonlinear fields are generated and detected, as shown in Fig. 3. We focus two

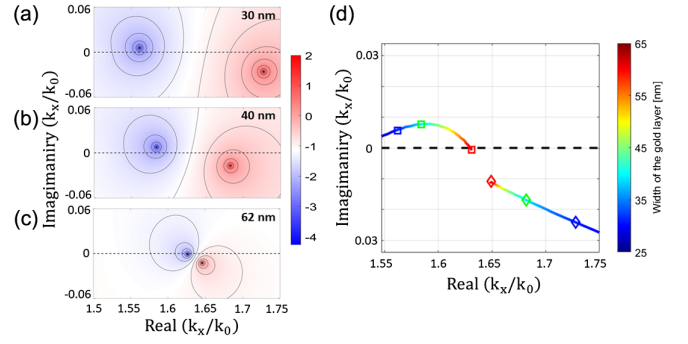


FIG. 2. Complex analysis of the generated nonlinear electric field (a)–(c). Calculated magnetic field (log scale) of resonant and antiresonant solutions in the presence of a nonlinear polarization for a gold layer of 30 nm (a), 40 nm (b), and 62 nm (c) and the variation of the resonant-antiresonant solutions with respect to the metallic width (left-right colored lines, respectively) (d). Fabricated metallic widths are marked as blue, green, and red squares (diamonds) indicate antiresonances (resonances) for 30, 40, and 62 nm gold layers, respectively.

TM-polarized laser pulses onto the gold surface. The pump pulse at $\lambda_a = 800$ nm was generated by a Ti:sapphire laser (Chameleon Ultra II, 140 fs pulses, repetition rate of 80 MHz) and a signal pulse generated by an adjacent optical parametric oscillator (Chameleon OPO) at $\lambda_b = 1000$ nm [Fig. 3(a)]. When spatial and temporal

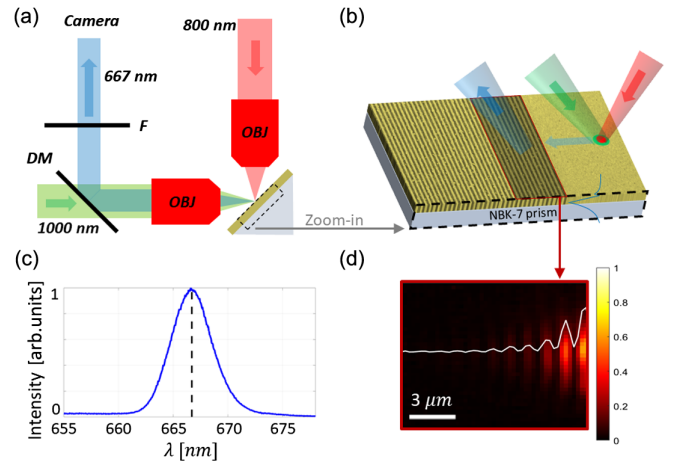


FIG. 3. Experimental concept: nonlinear generation and detection of short-range plasmons. (a) Pump (red) and signal (green) beams are focused onto a gold film using two long-working distance objectives oriented at $\pm 45^\circ$ to the surface. The scattered nonlinear field (blue) is separated by a dichroic mirror and a spectral filter and imaged onto a camera. (b) Nonlinearly generated resonant short-range plasmons (blue field profile) are scattered to the far field (blue arrows) by a grating (SEM image) milled all the way to the glass substrate using a focused ion beam. (c) The measured spectrum of the scattered field (blue curve) is centered on the expected PDFWM wavelength (dashed black line). (d) The measured image shows rapid decay of the scattered field (cross section in white corresponds to $3.3 \mu\text{m}$ decay length) that agrees with the calculated propagation distance of resonant short-range plasmon ($3.15 \mu\text{m}$).

overlap of the pulses are achieved, the third-order nonlinearity ($\chi^{(3)}$) of the gold film generates a nonlinear polarization at a wavelength of $\lambda_{nl} = 667$ nm [Fig. 3(c)]. The pump and signal incidence angles are selected such that the nonlinear polarization exhibits the required wave number of short-range plasmons (marked by the dashed circles in Supplemental Material Figs. 2S(a) and 2S(b) [36]). At such wave vectors, the nonlinear fields that provide access to the short-range plasmons do not radiate to the air or glass sides and, therefore, this process is referred to as *dark nonlinearity*. Hence, we use a scattering grating with a period of 729 nm to detect the nonlinear fields at the far field, following the relation

$$k_{x,nl}^s = k_{x,nl} + mK_g, \quad (3)$$

where $k_{x,nl}^s$ is the wave vector of the nonlinear field scattered by the grating, whose spatial frequency is $K_g = (2\pi/\Lambda)$ with Λ being the grating period. Taking $m = -1$ provides a scattering angle circa 45° .

We first illuminate the nonpatterned segment of the gold film in proximity to the grating, generating both resonant and antiresonant plasmons. Since antiresonant plasmons are restricted to the source location [26], only the resonant plasmon can propagate away from the illuminated region, reach the grating, and be scattered to the far field. Consequently, the intensity profile of the scattered nonlinear field, captured by the camera [Thorlabs DCC1545M, Fig. 3(d)], encapsulates the loss associated with the

resonant short-range plasmon. The measured intensity loss, quantified by $2\text{Im}(k_{SR})$, corresponds to about $3.3 \mu\text{m}$ decay length. This intensity attenuation is found to be in good agreement with the theoretical calculation, predicting an intensity decay length of $3.15 \mu\text{m}$. The measured spectrum of the scattered beam [Fig. 3(c)] indicates that it is indeed the nonlinear field that is captured, and its plasmonic nature is validated by the lack of a scattered nonlinear field when the polarization of the pump beam is switched to TE.

Being inhomogeneous solutions of the system, the antiresonant plasmons are obliged to a source and therefore can only be accessed via direct illumination. Consequently, driving the generation of the nonlinear source field at the grating location allows the detection of both the resonant and antiresonant field solutions by measuring and analyzing the scattered fields.

A prerequisite to observe these signatures is spanning a spatial frequency bandwidth covering both resonant and antiresonant plasmon wave vectors. This condition is naturally satisfied when focused beams are used to generate the sufficiently strong nonlinear polarization. The wave-vector range of the nonlinear field we generate is particularly broad due to the emerging convolution between the pump and signal beams $\sigma_{nl} = \sigma_a^* \sigma_b^*$, where σ_i is the spatial bandwidth of the pump (a), signal (b), and nonlinear (nl) fields [illustrated in Fig. 4(b)]. The scattering grating folds this wave-vector range across the light line, converting it into the spatial range of radiating waves we detect. We clearly observe pronounced peak-and-dip signatures in the spatial

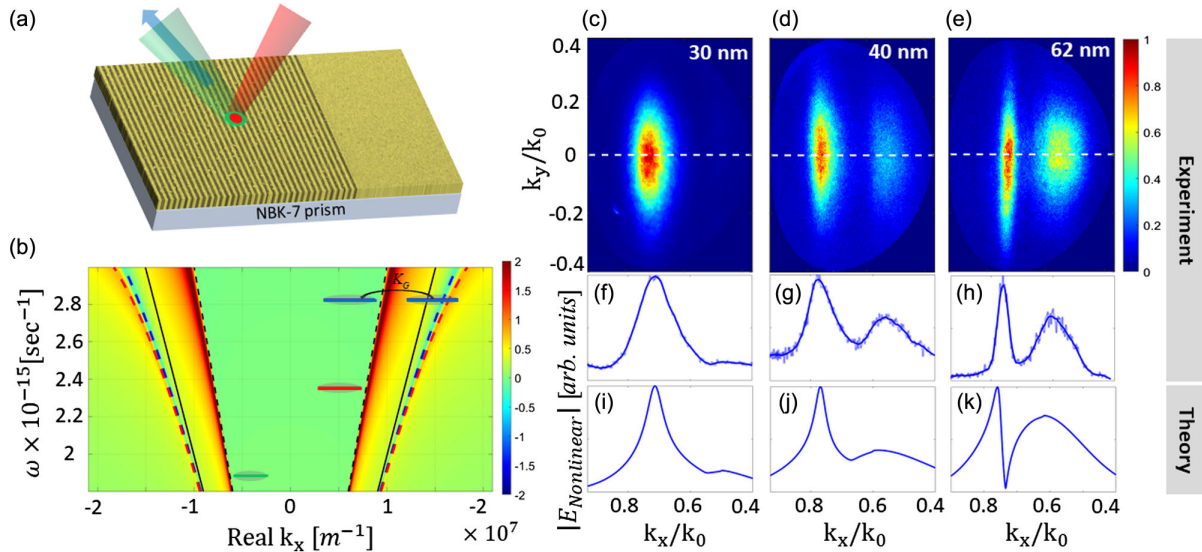


FIG. 4. Measurements of the nonlinear scattered fields. (a) An SEM image with an illustration of the nonlinear interaction. (b) Reflection coefficient displayed in a logarithmic scale [as in Fig. 1(a)] overlaid with an illustrated spatial extent of the pump and signal beams (red and green lines, respectively) and the detected extent of the nonlinear generation together with the scattered first order of diffraction (blue lines). The air light line, prism light line, resonant, and antiresonant dispersion curves are indicated by dashed black, black, dashed red, and dashed blue lines respectively. Measured nonlinear intensities in the reciprocal plane for a metallic width of 30 nm (c), 40 nm (d), and 62 nm (e) complemented with their corresponding norm cross sections along the k_x direction ($k_y = 0$) (f)–(h) and simulations (i)–(k), respectively.

emission spectrum, marking the excitation of both resonant and antiresonant short-range plasmons.

Figures 4(f)–4(h) depict the spatial emission spectrum of the scattered nonlinear field for gold film thicknesses of 30, 40, and 62 nm (the thicknesses are determined by ellipsometry). The film thickness dramatically affects the spatial spectra of the forced nonlinear emission, which transforms from a signature dominated by the resonant short-range plasmon (broad peak) to one that is shared by both resonant-antiresonant short-range plasmon pair (narrow dip and peak). The measured spectra are in agreement with the predicted spectra [Figs. 4(i)–4(k)] whose calculation is detailed in the Supplemental Material. It should be noted that as the thickness of the metallic layer is increased even further the metallic layer can be considered as a semi-infinite slab and should not exhibit resonant-antiresonant state pairs.

To conclude, we leveraged a form of nonradiating nonlinear polarization (dark nonlinearity) to access and observe, for the first time, resonant-antiresonant pairs of short-range plasmons. Exploiting the nonlinear polarization as a source in the near field, we derived the dependence of these two distinct plasmonic variants on film thickness and found conditions under which nonlinearity-driven direct coupling to antiresonant short-range plasmons takes place—a condition that is unattainable with linear excitation of thin films. Exploiting SR plasmonic states may provide a powerful and enabling tool which can be harnessed for refractive index sensing of buried dielectrics or for novel subwavelength resolution microscopy schemes.

Our findings open a path to design novel nanophotonic devices and applications, in which modal and nonmodal states and their properties are accurately controlled by a nonlinear source. In particular, controlling the losses of an antiresonant state has been detrimental to several recent applications, such as low-loss propagation in hollow core optical fibers [27,28] and antilasing in cavities [29] or disordered media [37]. Moreover, the generality of our method and analysis may be utilized for other forms of surface states in plasmonic, phononic, or excitonic materials or guided waves in optical waveguides or photonic crystals where nonlinear parametric processes like sum or difference frequency generation or Kerr-type nonlinearities may provide a unique and sensitive ability to control both modal and nonmodal state pairs.

This work was supported by the Israel Science Foundation (ISF) Grant No. 1750/18 and the Russell Berrie Nanotechnology Institute (RBNI) at the Technion. We acknowledge help provided in sample fabrication by the photovoltaic laboratory and the Micro-Nano Fabrication unit (MNFU) at the Technion, especially by Dr. G. Ankonina and Dr. L. Popilevsky. S. T. acknowledges support by the Adams Fellowship Program of the Israel Academy of Science and Humanities.

- [1] N. Bloembergen and P. S. Pershan, *Phys. Rev.* **128**, 606 (1962).
- [2] F. Brown, R. E. Parks, and A. M. Sleeper, *Phys. Rev. Lett.* **14**, 1029 (1965).
- [3] S. S. Jha, *Phys. Rev. Lett.* **15**, 412 (1965).
- [4] R. K. Chang and N. Bloembergen, *Phys. Rev.* **144**, 775 (1966).
- [5] N. Bloembergen, W. K. Burns, and M. Matsuoka, *Opt. Commun.* **1**, 195 (1969).
- [6] M. Fleischmann, P. J. Hendra, and A. J. McQuillan, *Chem. Phys. Lett.* **26**, 163 (1974).
- [7] D. L. Jeanmaire and R. P. Van Duyne, *J. Electroanal. Chem.* **84**, 1 (1977).
- [8] H. J. Simon, D. E. Mitchell, and J. G. Watson, *Phys. Rev. Lett.* **33**, 1531 (1974).
- [9] S. Kim, J. Jin, Y. J. Kim, I. Y. Park, Y. Kim, and S. W. Kim, *Nature (London)* **453**, 757 (2008).
- [10] E. Almeida and Y. Prior, *Sci. Rep.* **5**, 10033 (2015).
- [11] G. Vampa, B. G. Ghamsari, S. Siadat Mousavi, T. J. Hammond, A. Olivieri, E. Lisicka-Skrek, A. Y. Naumov, D. M. Villeneuve, A. Staudte, P. Berini, and P. B. Corkum, *Nat. Phys.* **13**, 659 (2017).
- [12] E. Almeida, G. Shalem, and Y. Prior, *Nat. Commun.* **7**, 10367 (2016).
- [13] E. Almeida, O. Bitton, and Y. Prior, *Nat. Commun.* **7**, 12533 (2016).
- [14] S. Palomba, S. Zhang, Y. Park, G. Bartal, X. Yin, and X. Zhang, *Nat. Mater.* **11**, 34 (2012).
- [15] K. Frischwasser, K. Cohen, J. Kher-Alden, S. Dolev, S. Tsesses, and G. Bartal, *Nat. Photonics* **15**, 442 (2021).
- [16] H. Raether, G. Hohler, and E. A. Niekisch, *Springer Tracts Mod. Phys.* **111**, 136 (1988).
- [17] S. A. Maier, *Plasmonics: Fundamentals and Applications* (Springer, New York, 2007).
- [18] S. Palomba and L. Novotny, *Phys. Rev. Lett.* **101**, 056802 (2008).
- [19] J. Renger, R. Quidant, N. Van Hulst, S. Palomba, and L. Novotny, *Phys. Rev. Lett.* **103**, 266802 (2009).
- [20] J. Renger, R. Quidant, N. Van Hulst, and L. Novotny, *Phys. Rev. Lett.* **104**, 046803 (2010).
- [21] N. B. Grosse, J. Heckmann, and U. Woggon, *Phys. Rev. Lett.* **108**, 136802 (2012).
- [22] T. J. Constant, S. M. Hornett, D. E. Chang, and E. Hendry, *Nat. Phys.* **12**, 124 (2016).
- [23] E. N. Economou, *Phys. Rev.* **182**, 539 (1969).
- [24] J. J. Burke, G. I. Stegeman, and T. Tamir, *Phys. Rev. B* **33**, 5186 (1986).
- [25] M. N. Zervas, *Opt. Lett.* **16**, 720 (1991).
- [26] G. Rosenblatt, B. Simkhovich, G. Bartal, and M. Orenstein, *Phys. Rev. X* **10**, 011071 (2020).
- [27] F. Poletti, *Opt. Express* **22**, 23807 (2014).
- [28] H. Sakr, Y. Chen, G. T. Jasion, T. D. Bradley, J. R. Hayes, H. C. H. Mulvad, I. A. Davidson, E. Numkam Fokoua, and F. Poletti, *Nat. Commun.* **11**, 6030 (2020).
- [29] Z. J. Wong, Y. L. Xu, J. Kim, K. O'Brien, Y. Wang, L. Feng, and X. Zhang, *Nat. Photonics* **10**, 796 (2016).
- [30] G. Rosenblatt and M. Orenstein, *Phys. Rev. Lett.* **115**, 195504 (2015).
- [31] R. W. Boyd, *Nonlinear Optics* (Elsevier Inc., New York, 2008).

- [32] E. Almeida and Y. Prior, *Sci. Rep.* **5**, 10033 (2015).
- [33] D. S. Bethune, *J. Opt. Soc. Am. B* **6**, 910 (1989).
- [34] A. Rose, S. Larouche, D. Huang, E. Poutrina, and D. R. Smith, *Phys. Rev. E* **82**, 036608 (2010).
- [35] X. Liu, A. Rose, E. Poutrina, C. Ciraci, S. Larouche, and D. R. Smith, *J. Opt. Soc. Am. B* **30**, 2999 (2013).
- [36] See Supplemental Material at <http://link.aps.org/supplemental/10.1103/PhysRevLett.128.103901> for theoretical details.
- [37] K. Pichler, M. Kühmayer, J. Böhm, A. Brandstötter, P. Ambichl, U. Kuhl, and S. Rotter, *Nature (London)* **567**, 351 (2019).